Electronic Supplementary Material (ESI) for Journal of Materials Chemistry A.

SUPPORTING INFORMATION

Multi-length Scale 5D Diffraction Imaging of Ni-Pd/CeO_2-ZrO_2/Al_2O_3 Catalyst during Partial Oxidation of Methane

Dorota Matras[1,2*], Antonios Vamvakeros[3,4,5], Simon D. M. Jacques[3*], Marco di Michiel[4], Vesna Middelkoop[6], Ilyas Z. Ismagilov[7], Ekaterina V. Matus[7], Vadim V. Kuznetsov[7], Robert J. Cernik[1] and Andrew M. Beale [2,3,5*]

[1] School of Materials, University of Manchester, Manchester, Lancashire M13 9PL, UK.

[2] Research Complex at Harwell, Harwell Science and Innovation Campus, Rutherford Appleton Laboratory, Didcot, Oxon, OX11 0FA, UK.

[3] Finden Limited, Merchant House, 5 East St Helen Street, Abingdon, OX14 5EG, UK.

[4] ESRF- The European Synchrotron, Grenoble, 38000 France.

[5] Department of Chemistry, University College London, 20 Gordon Street, London, WC1H 0AJ, UK.

[6] Flemish Institute for Technological Research, VITO NV, Boeretang 200, 2400 Mol, Belgium.

[7] Boreskov Institute of Catalysis SB RAS, Pr. Akademika Lavrentieva 5, 630090 Novosibirsk, Russia.

Correspondance email: dorota.matras@rc-harwell.ac.uk, simon@finden.co.uk, andrew.beale@ucl.ac.uk.

1. Experimental information

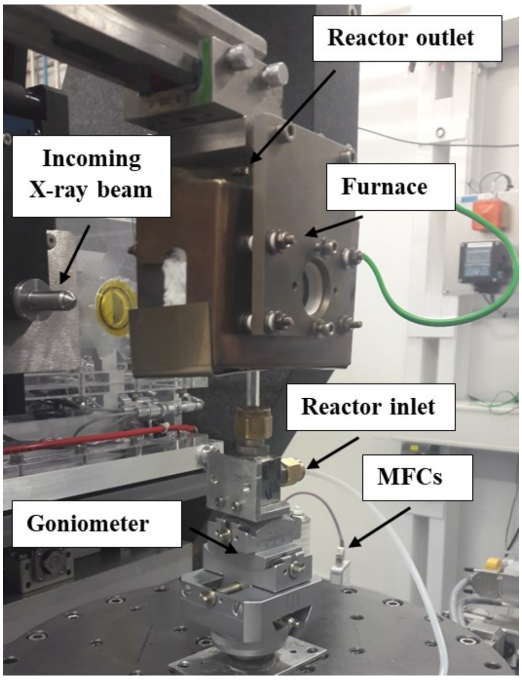

Figure S1. *Photograph of experimental set up used at the beamline ID15A, ESRF.*

Note that in order to probe the entire catalyst bed with XRD mapping the motorised z stage, where the reactor is mounted on, needs to be moved in z direction accordingly. This results in parts of the catalyst bed (i.e. bottom/reactor inlet) being exposed to different temperatures, however at the point of measurement (line scans in XRD map or XRD-CT cross section) the temperature is assumed to be isothermal.

Table S1. *Crystallographic information about all the identified phases.*

Phase	Crystallographic details	ICSD database code
NiO	cubic, Fm-3m	28834
CeO_2	cubic, Fm-3m	88759
ZrO_2	tetragonal, P42/nmcZ	66781
PdO	tetragonal, P42/mmc	24692
Al_2O_3	monoclinic, A2/n	generated by Kovarik et al. [1]

Pd-Ni	**cubic, Fm-3m**	**105307**
$NiAl_2O_4$	cubic, Fd-3mZ	9556
Ni	cubic, Fm-3m	64989
Graphite	hexagonal, R-3mR	31829

2. Solid-state chemistry at room temperature

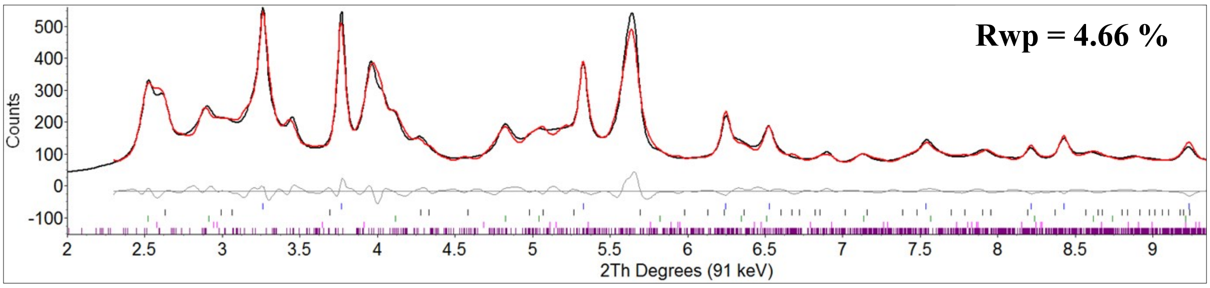

Figure S2. *Results of the Rietveld refinement analysis on diffraction pattern collected at room temperature (from the middle of 3D-XRD-CT dataset- 5th XRD-CT scan).*

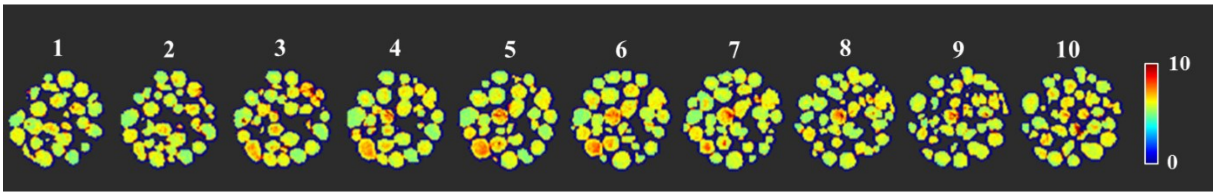

Figure S3. *Results of Rwp errors obtained from the Rietveld refinement analysis of XRD-CT data collected at room temperature. Numbers above the images corresponds to position in the 3D-XRD-CT data volume, presented towards the outlet/top of the reactor.*

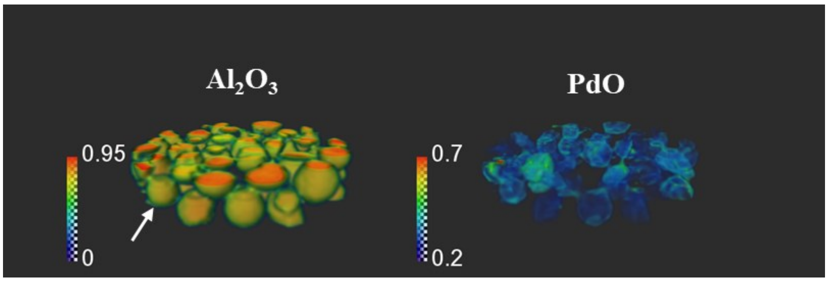

Figure S4. *Volume rendering of the normalised scale factors data volume (normalised over the maximum value of the scale factor in the entire process) obtained from the Rietveld analysis of the 3D-XRD-CT data collected at room temperature for Al_2O_3 and PdO. White arrow on the Al_2O_3 volumes shows the catalyst particle used for the expansion analysis presented in the further section of Supporting Information.*

3. Solid-state chemistry during temperature ramp under He

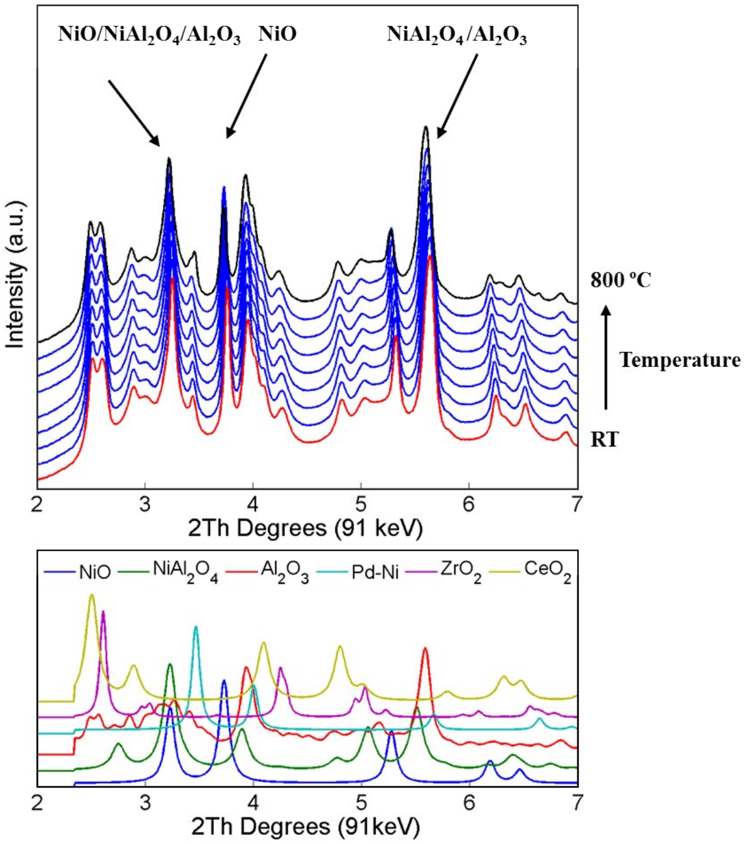

Figure S5. *Top: diffraction patterns showing the evolution of solid-state chemistry in the catalyst bed at the outlet of reactor collected during the temperature ramp from room* *temperature to 800 °C and under He. Red line corresponds to a diffraction pattern collected at the room temperature and the black line corresponds to a diffraction pattern collected at 800 ºC. Bottom: simulated diffraction patterns for all crystalline phases present at 800 °C.*

It is important to note that due to the overlapping reflections between $NiAl_2O_4$, Al_2O_3 and NiO the only visible changes (in the presented diffraction patterns) are related to peak broadening, which suggest formation of an additional phase (i.e. $NiAl_2O_4$) at high temperatures.

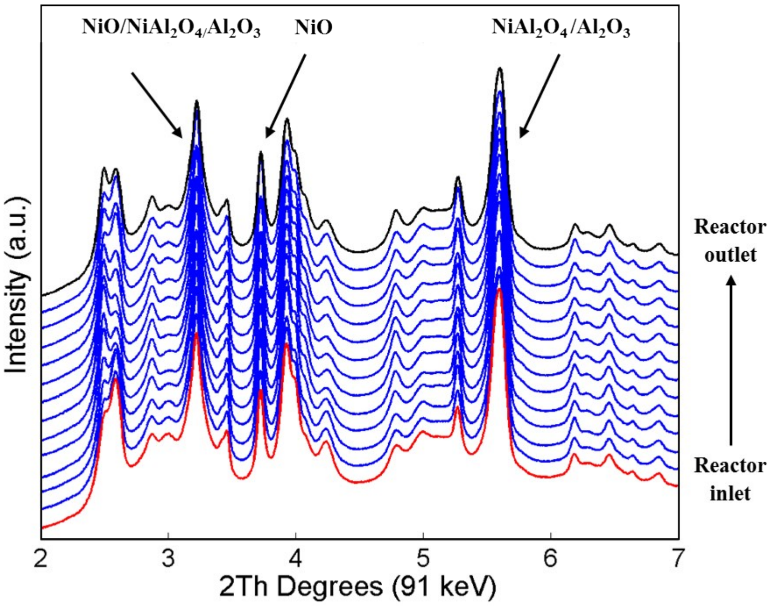

Figure S6. *Diffraction pattern showing the evolution of solid-state chemistry collected during the last XRD map at temperatures above 780 °C and under He (one XRD map lasted ~ 5 min). Red line corresponds to a line scan collected at the reactor inlet and the black line corresponds to a line scan collected at the reactor outlet.*

In the last XRD map collected at temperatures above 780 °C no gradient between $NiAl_2O_4$ and NiO phases can be observed along the catalyst bed.

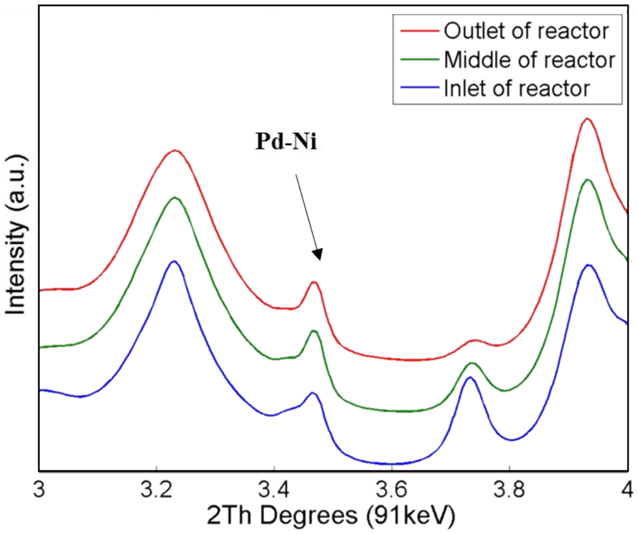

Figure S7. *Diffraction pattern showing the peak of mixed Pd-Ni phase (black arrow) collected during the XRD-CT measurements at 800 °C and under He (one XRD-CT scan lasted for ~ 9 min). Red line corresponds diffraction pattern from XRD-CT measurement at the inlet of reactor, blue line corresponds diffraction pattern from XRD-CT measurement at the middle of reactor and finally black line corresponds to diffraction pattern from XRD-CT measurement at the outlet of reactor.*

As shown in Figure S7, no apparent peak shift of the Pd-Ni phase can be observed for the three diffraction patterns collected from different parts of reactor. This result suggests that the composition of the metallic Pd-Ni alloy does not change along the bed and as a function of time. In addition, the decrease in intensity of the NiO peak is due to the interaction of NiO with Al_2O_3 support; the apparent gradient between reactor inlet and reactor outlet is due to the time of measurements (~ 9 min per XRD-CT image and data collected from reactor inlet to reactor outlet).

4. Scanning electron microscopy and elemental analysis mapping

The scanning electron microscopy measurements on the cross section of catalyst particles, coupled with energy dispersive X-ray spectrometry (SEM-EDX) were performed using the FEI

Nova NanoSEM 450 scanning electron microscope with an ultrastable, high current Schottky field-emission source, fitted with an EDX detectors and using an accelerating voltage of 20 kV.

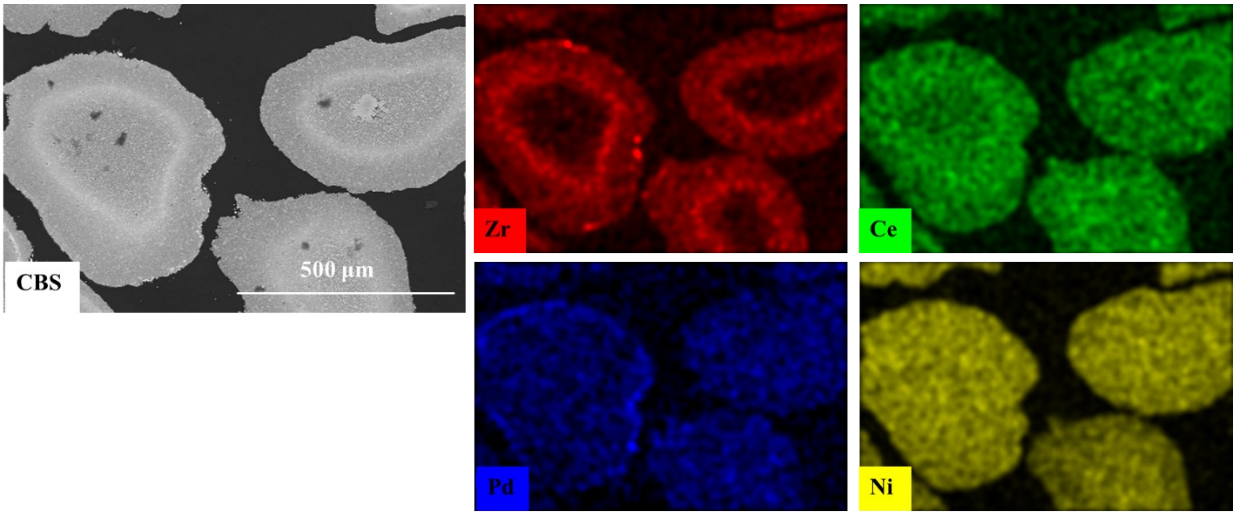

Figure S8. *SEM and EDX mapping of the Ni-Pd/CeO_2-ZrO_2/Al_2O_3 fresh catalyst cross section.*

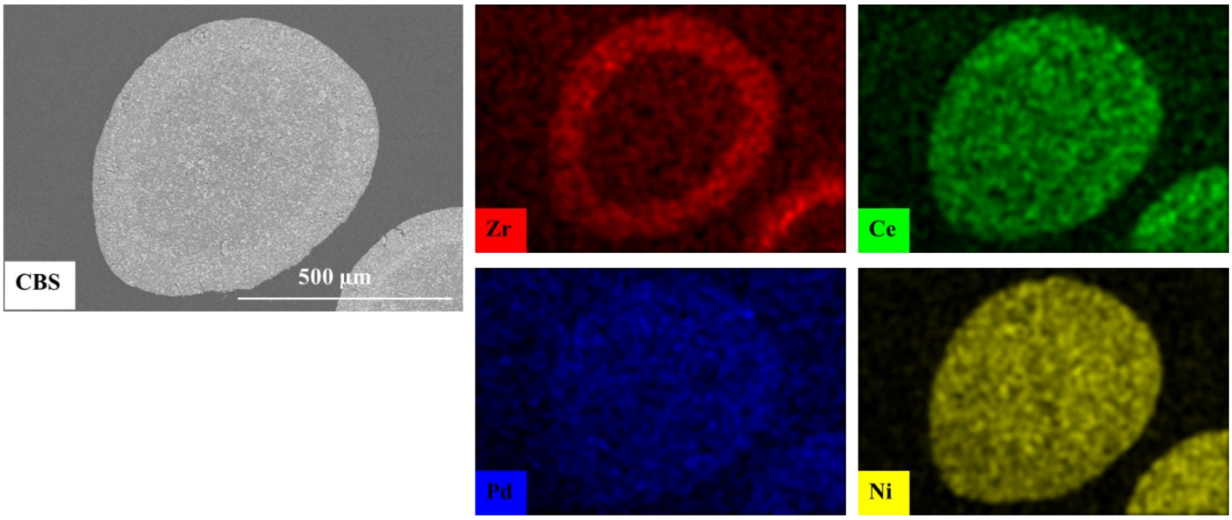

Figure S9. *SEM and EDX mapping of the Ni-Pd/CeO_2-ZrO_2/Al_2O_3 catalyst cross section recovered after the POX reaction.*

5. Solid-state chemistry during the reduction process

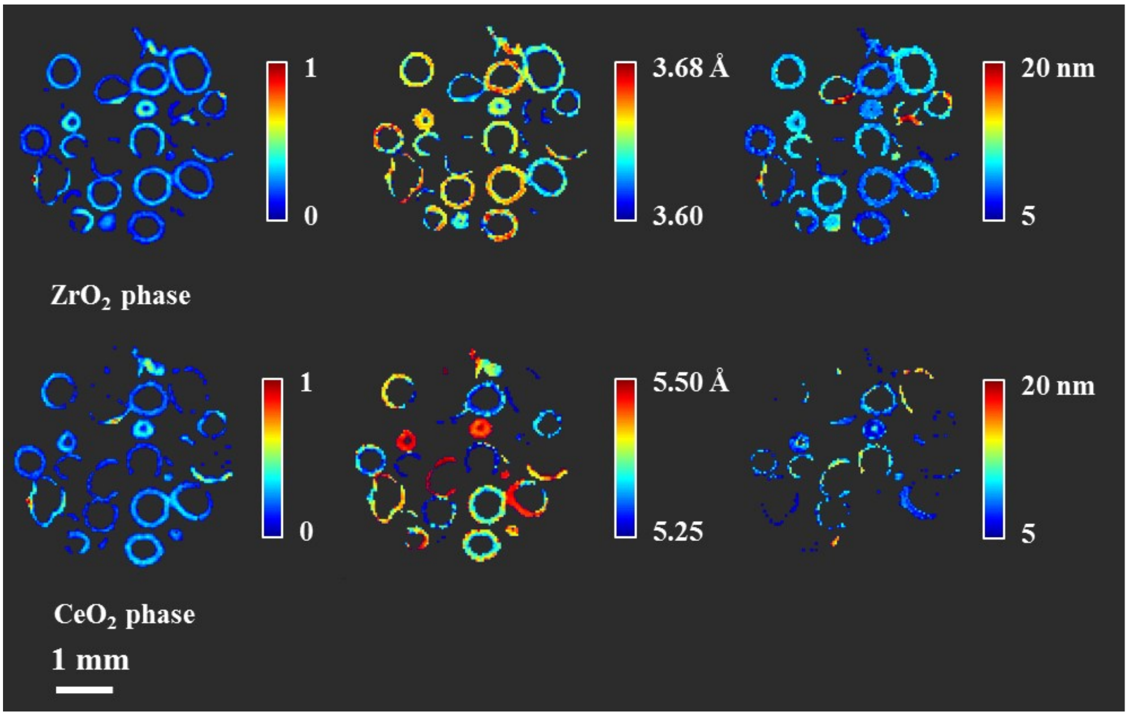

Figure S10. *Spatial distribution of normalised scale factor (in respect to maximum value in this XRD-CT image), spatial distribution of crystallite size and lattice parameter a for* CeO_2 *and* ZrO_2 *collected during the reduction.*

A significant change in the distribution of CeO_2 occurred during the reduction of catalyst. CeO_2 previously present in the core of catalyst particle disappeared and its distribution at this stage became very similar to ZrO_2, meaning that regions of pure CeO_2 phase are not any more present in the catalyst particle. As mentioned in the main text, the disappearance of CeO_2 from the core of catalyst particles may be due to the reaction between CeO_2 and Al_2O_3 support and formation of another phase $CeAlO_3$. However, no reflections associated to this phase could be detected with diffraction. The fact that CeO_2 is seen to significantly decrease from the core of catalyst (rich in Al_2O_3) may be the correct reasoning confirming the formation of $CaAlO_3$. The distribution of ZrO_2 was not affected during the reduction treatment and no significant changes related to ZrO_2 crystallite or lattice parameter *a* were seen.

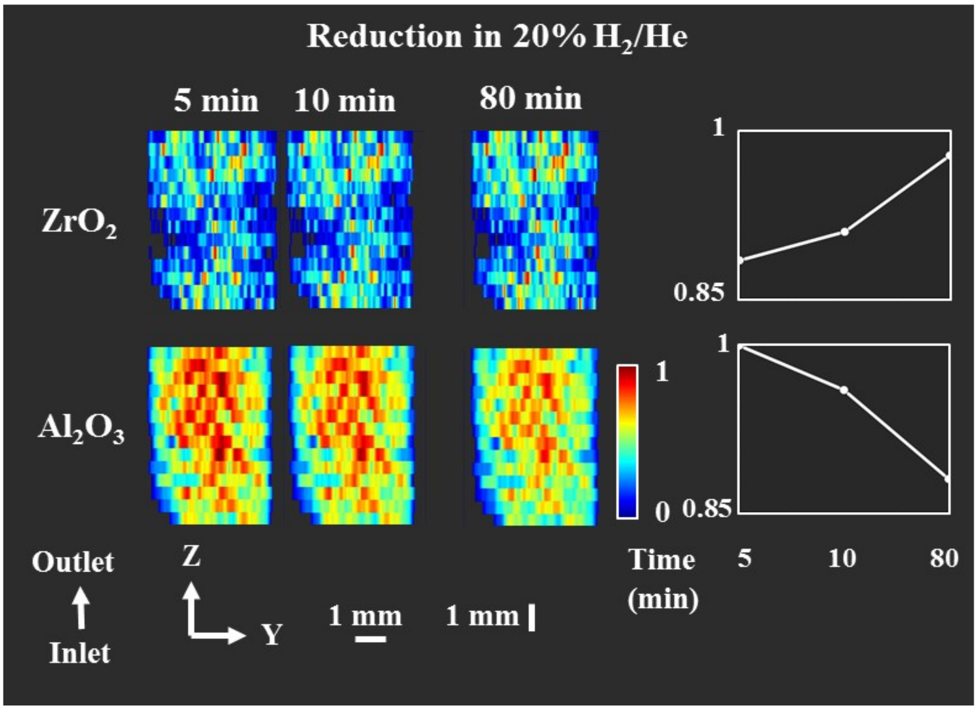

Figure S11. *Phase distribution maps of ZrO_2 and Al_2O_3, corresponding to the normalized scale factors obtained through Rietveld analysis of the XRD maps collected during reduction step. Right: relative changes of each phase during the reduction step. XRD maps are presented from the inlet of reactor towards the outlet of reactor.*

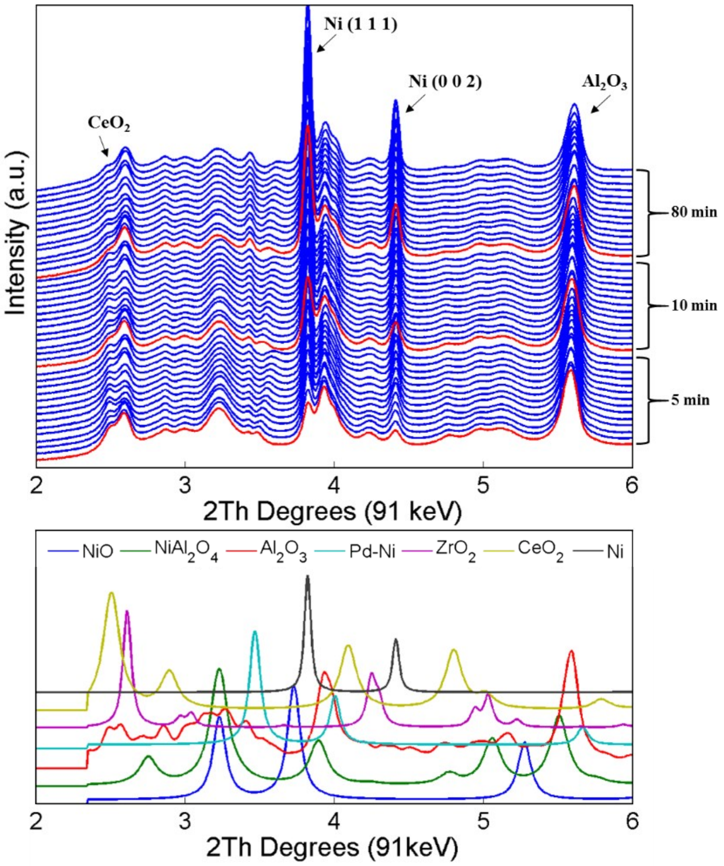

Figure S12. *Top: summed diffraction patterns collected with diffraction mapping (summed line scan) during the reduction: first two sets correspond to XRD map collected during 5 and 10 minutes and the last set corresponds to XRD map collected after 80 minutes of reduction. Red line presents the beginning of each map and the data are presented from the inlet of reactor towards the outlet of reactor. Arrows indicated reflections from* CeO_2 *and metallic Ni phase. Bottom: simulated diffraction patterns for all crystalline phases present during reduction at 800 °C.*

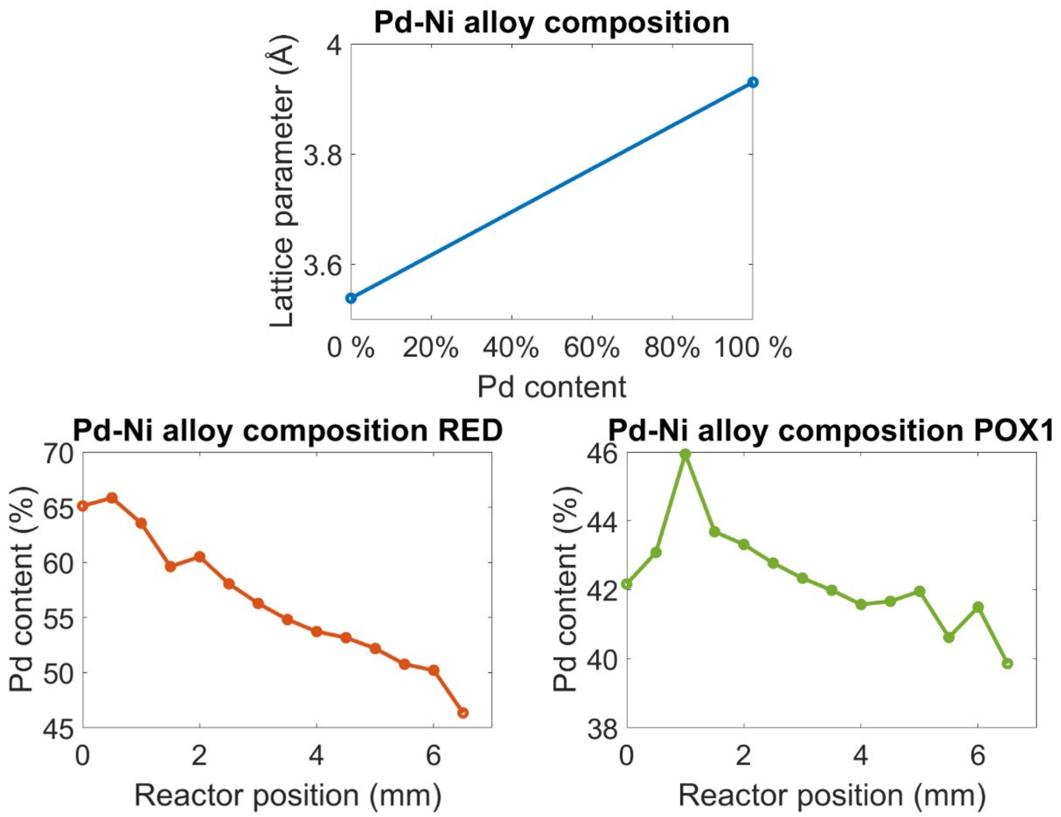

Figure S13. *Top: Pd-Ni alloy composition calculated using the Vegard's law (Pd lattice parameter was taken from* [2] *and Ni lattice parameter was calculated from the experimental data in this study). Bottom left: Pd-Ni alloy composition as a function of catalyst bed position during reduction (XRD map collected after 80 min of reduction, Figure 6 in the main manuscript). Bottom right: Pd-Ni alloy composition as a function of catalyst bed position during POX1 (XRD map collected after 80 min of POX1 reaction, Figure 8 in the main manuscript).*

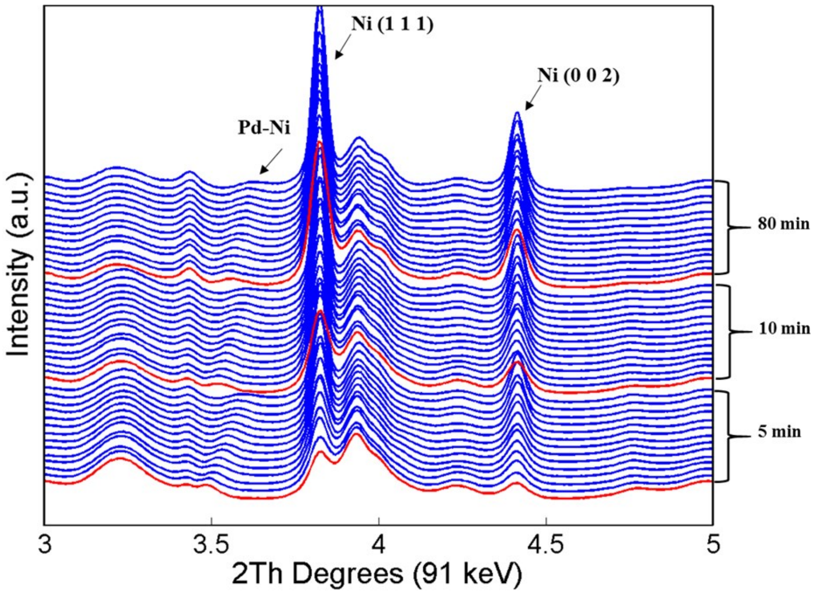

Figure S14. *Summed diffraction patterns collected with diffraction mapping (summed line scan) during the reduction: first two sets correspond to XRD map collected during 5 and 10 minutes and the last set corresponds to XRD map collected after 80 minutes of reduction. Red line presents the beginning of each map and the data are presented from the inlet of reactor towards the outlet of reactor. Arrows indicated reflections from Pd-Ni and metallic Ni phase.*

The reflection of Pd-Ni shifts towards higher 2θ values (smaller lattice parameter a) when passing from inlet of reactor to outlet of reactor. Regarding the metallic Ni phase, broader peaks can be observed at the inlet of reactor and when passing to outlet of reactor peaks become sharper. All these observations are related to bed height and not to time on stream.

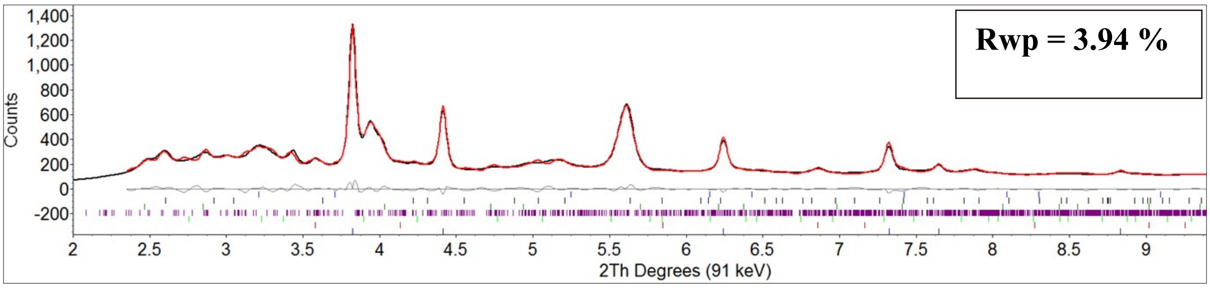

Figure S15. *Results of the Rietveld refinement analysis on diffraction pattern collected during the reduction (from the middle of 3D-XRD-CT dataset- 5th XRD-CT scan).*

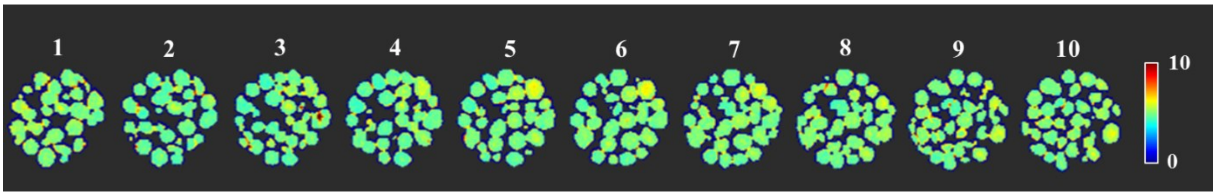

Figure S16. *Results of R_{wp} errors obtained from the Rietveld refinement analysis of XRD-CT data collected during reduction. Numbers above the images corresponds to position in the 3D-XRD-CT data volume, presented towards the outlet/top of the reactor.*

6. Solid-state changes and catalyst performance during the partial oxidation of methane reaction

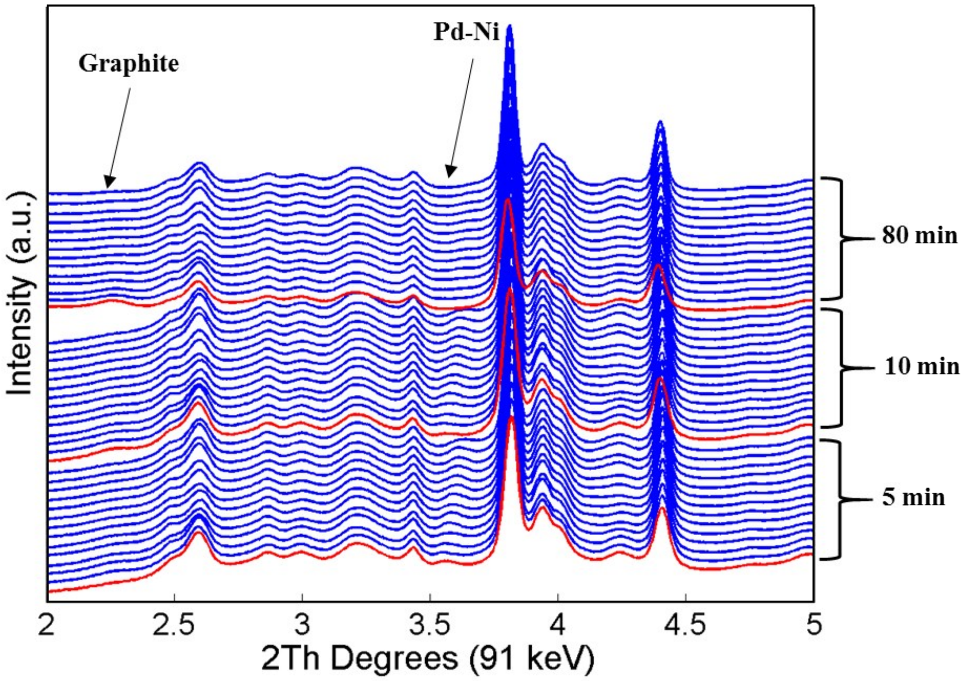

Figure S17. *Summed diffraction patterns collected with diffraction mapping (summed line scan) during the reaction mixture POX1: first two sets correspond to XRD map collected during 5 and 10 minutes and the last set corresponds to XRD map collected after 80 minutes of POX reaction. Red line presents the beginning of each map and the data are presented from the inlet of reactor towards the outlet of reactor. Arrows indicated reflections from Pd-Ni and graphite.*

During the first 10 minutes of POX1 reaction mixture, the reflection of Pd-Ni shifts towards higher 2θ values (smaller lattice parameter) when passing from inlet of reactor to outlet of reactor. After 80 minutes of POX1 reaction mixture, the reflection of Pd-Ni disappeared, which is coincident with the appearance of graphite diffraction peak.

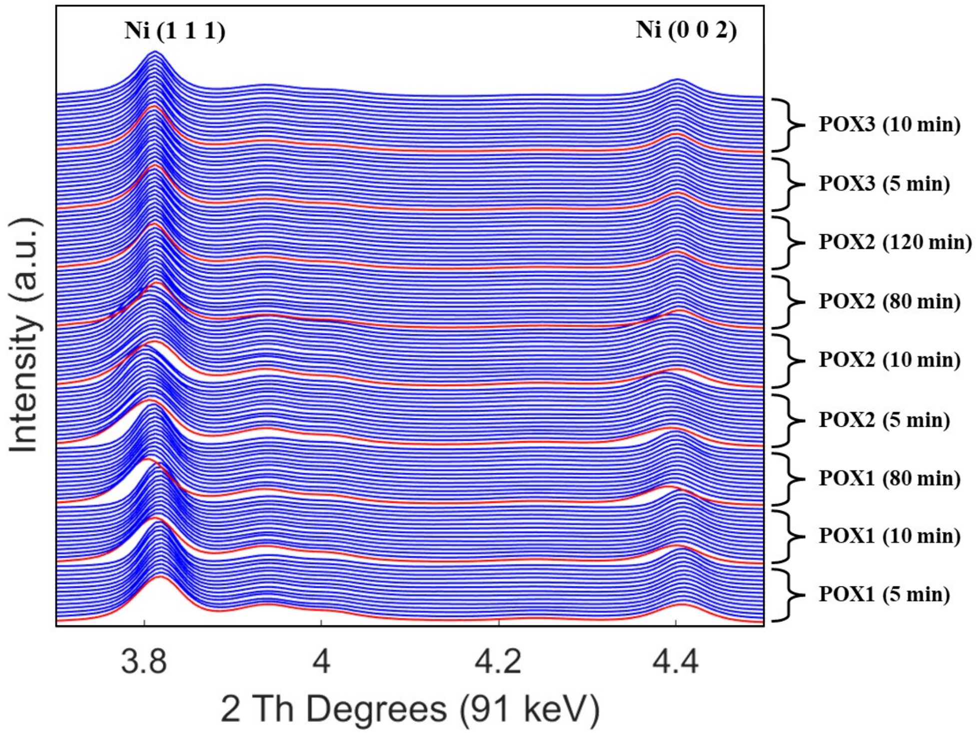

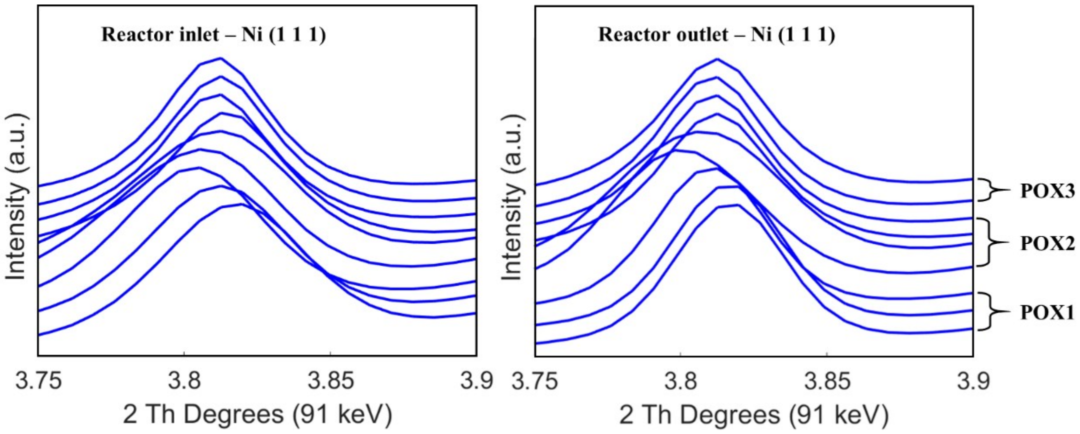

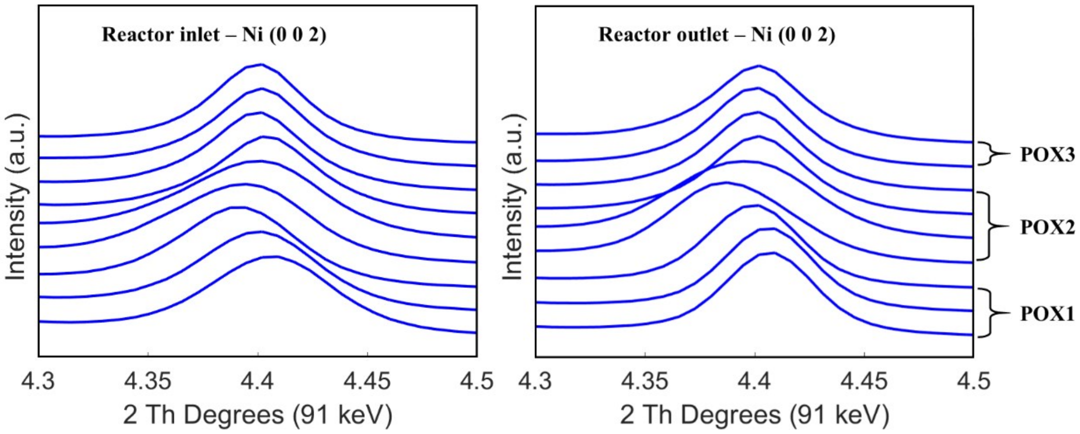

Figure S18. *Top panel: Summed diffraction patterns collected with diffraction mapping (summed line scan) during the reaction mixture POX1, POX2 and POX3. Red line presents the beginning of each map and the data are presented from the inlet of reactor towards the outlet of reactor. Middle panel: summed diffraction patterns corresponding to the Ni (1 1 1) reflection collected with diffraction mapping (summed diffraction pattern per line scan) during the reaction mixture POX1, POX2 and POX3 for the reactor inlet and the rector outlet. Bottom panel: summed diffraction patterns corresponding to the Ni (0 0 2) reflection collected with diffraction mapping (summed diffraction pattern per line scan) during the reaction mixture POX1, POX2 and POX3 for the reactor inlet and the rector outlet.*

The catalyst sample (500 mg) was heated under atmosphere of He to 800 °C with a ramp rate of 20 °C·min^{-1}. Dwell of 30 min under He flow was applied before switching to reducing conditions. In this reduction step, the catalyst was reduced under the flow 10 % H_2/He (H_2/He = 1/ 9, with total flow 100 sccm) for 1 h. After this activation step, the first POX reaction mixture of CH_4/O_2/He = 2/1/1.5 with total flow 240 sccm ((GHSV of 480,000 mL·min^{-1}·g^{-1}) was tested in the reactor for 2 h. After that, the second POX reaction mixture of CH_4/O_2/He = 4/1/3 with total flow 220 sccm (GHSV of 440,000 mL·min^{-1}·g^{-1}) was introduced and tested for 3 h. Finally, the last POX reaction mixture introduced to reactor was identical with the first POX reaction mixture and was tested for 1 h.

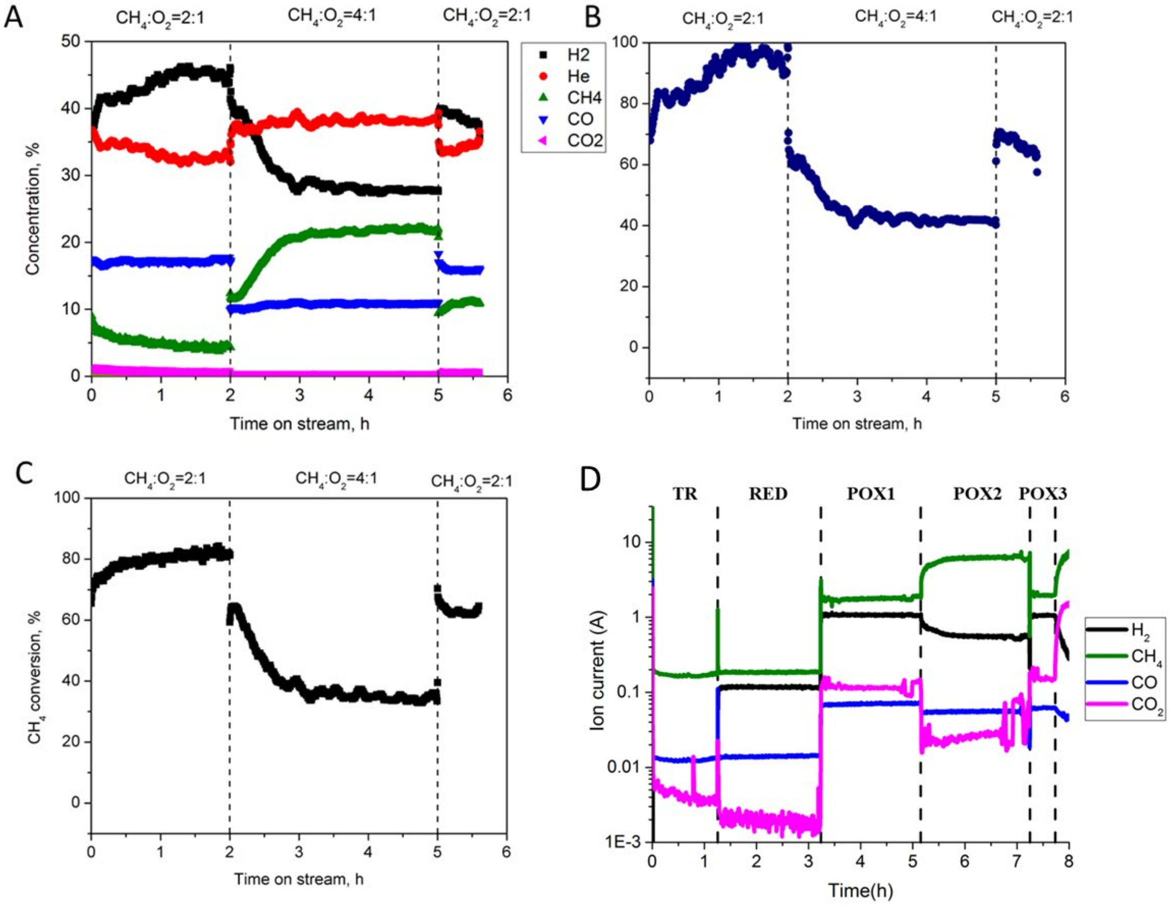

Figure S19: *Results of laboratory tests measurements and results of mass spectrometry collected during the operando synchrotron experiment. Panel A: concentration of reactants and products as a function of time, panel B: H_2 yield as a function of time and panel C: CH_4 conversion as a function of time* [3]*, panel D: mass spectrometry signal collected during the various stages of the operando experiment: TR - temperature ramp, RED - reduction, POX1 reaction mixture, POX2 reaction mixture and POX3 reaction mixture; signal of all components was normalised in respect to signal of He.*

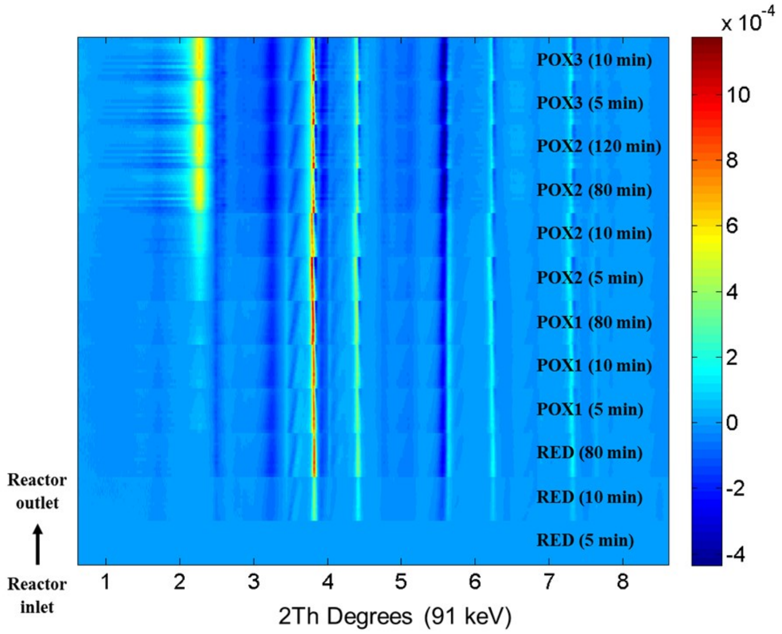

Figure S20. *Relative changes in the background of collected diffraction patterns with XRD mapping measurements during various reaction stages (from reduction to POX3). Diffraction patterns obtained in the first XRD map – reduction 5 minutes were subtracted from the consecutive scans to follow the relative changes in the background. Diffraction patterns from XRD map are presented from reactor inlet towards the reactor outlet.*

From Figure S20 we observed that no significant changes in the diffraction patterns background occurred during the experiment (including the activation and POX reaction stages), which would exclude formation of amorphous carbon species.

Thermogravimetric analysis were performed using the TGA Q50 (TA Instruments). The spent catalyst sample (10 mg) was placed in the atmosphere of Air and the temperature was increased from ambient to 950 °C with temperature ramp of 5 °C·min^{-1}.

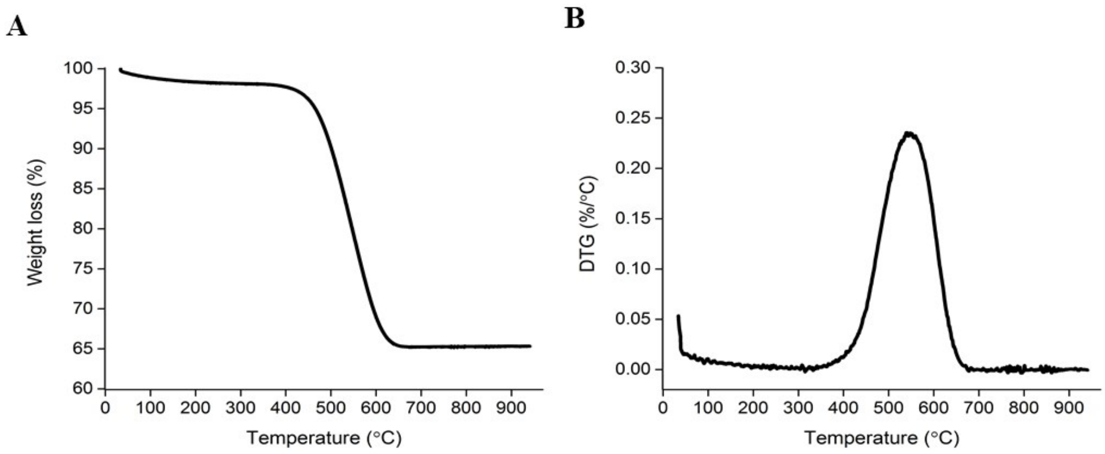

Figure S21. *Panel A: Results of thermogravimetric analysis performed on the spent sample of catalyst and panel B: results of differential thermogravimetric analysis performed on the spent sample of catalyst* [3].

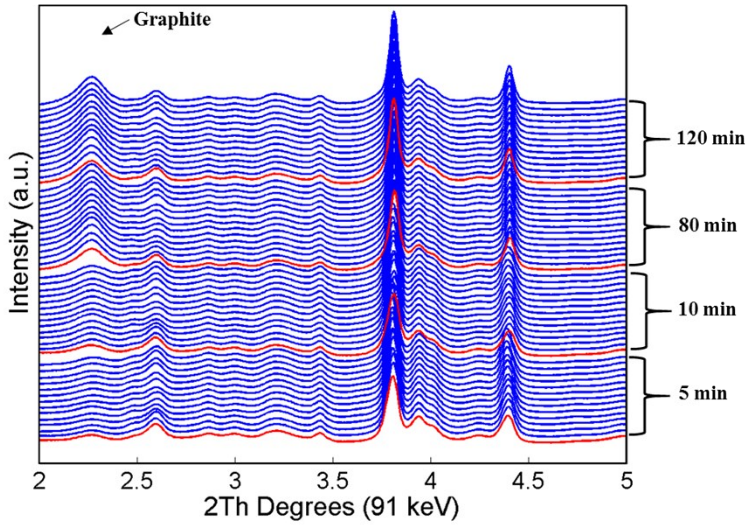

Figure S22. *Summed diffraction patterns collected with diffraction mapping (summed line scan) during the reaction mixture POX2: first two sets correspond to XRD map collected during 5 and 10 minutes, the third set corresponds to XRD map collected after 80 minutes of POX reaction and the last set corresponds to XRD map collected after 120 minutes of POX reaction. Red line presents the beginning of each map and the data are presented from the inlet of reactor towards the outlet of reactor. The arrow indicates graphite peak.*

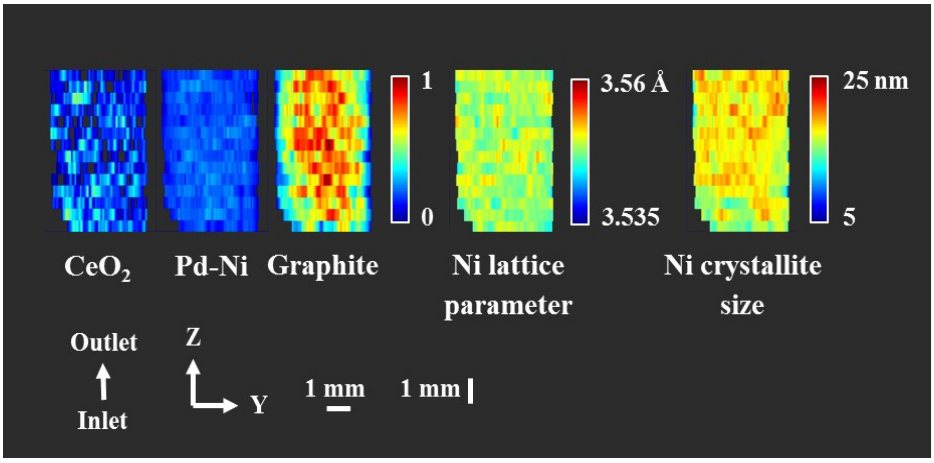

Figure S23. *Phase distribution maps of normalised scale factors for* CeO_2*,* Ni_xPd_y *and graphite, Ni lattice parameter and Ni crystallite size obtained through Rietveld analysis of the XRD maps collected during POX2 (80 minutes). XRD maps are presented from the inlet of reactor towards the outlet of reactor.*

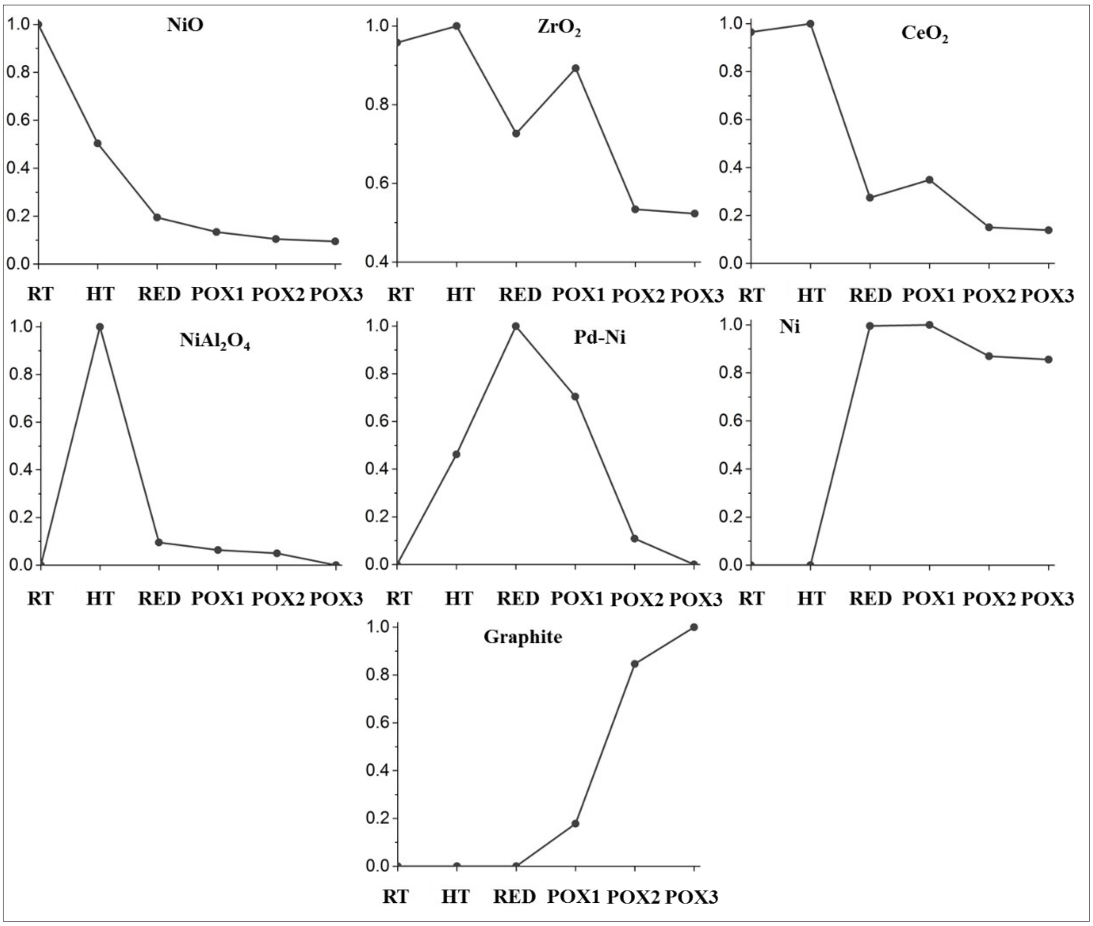

Figure S24. *Normalised scale factor (mean value for entire 3D XRD-CT volume data) for each crystalline phase present in catalyst during the POX experiment.*

According to the Rietveld analysis (Figure S25), the coke deposition was much more significant in the core of catalyst particles, rather than on their surface and this was due to the promoting effect of binary CeO_2-ZrO_2 solid solution. Its role was to supress the coke formation through the release of stored oxygen as well as due to the enhanced redox properties of this mixed phase. The difference map clearly illustrates that the coke formation was lower where the mixed CeO_2-ZrO_2 was present.

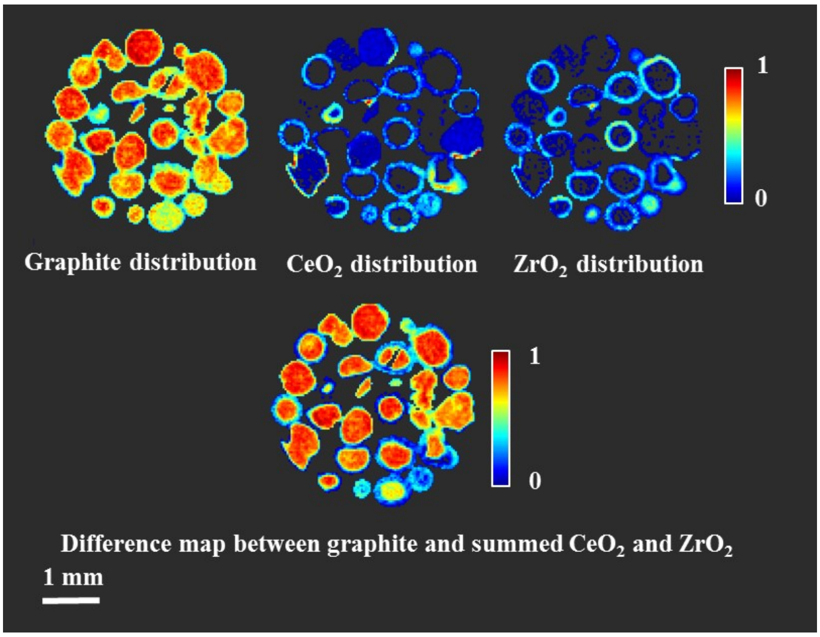

Figure S25. *Spatial distribution of normalised scale factors obtained through Rietveld refinement (in respect to maximum value in this XRD-CT image) for* ZrO_2*,* CeO_2 *and graphite collected reaction mixture POX2. The difference map was obtained through subtraction of summed and normalised* ZrO_2 *and* CeO_2 *distribution from normalised graphite distribution. The colorbar was chosen to emphasize the regions of catalyst particles where the graphite phase grew.*

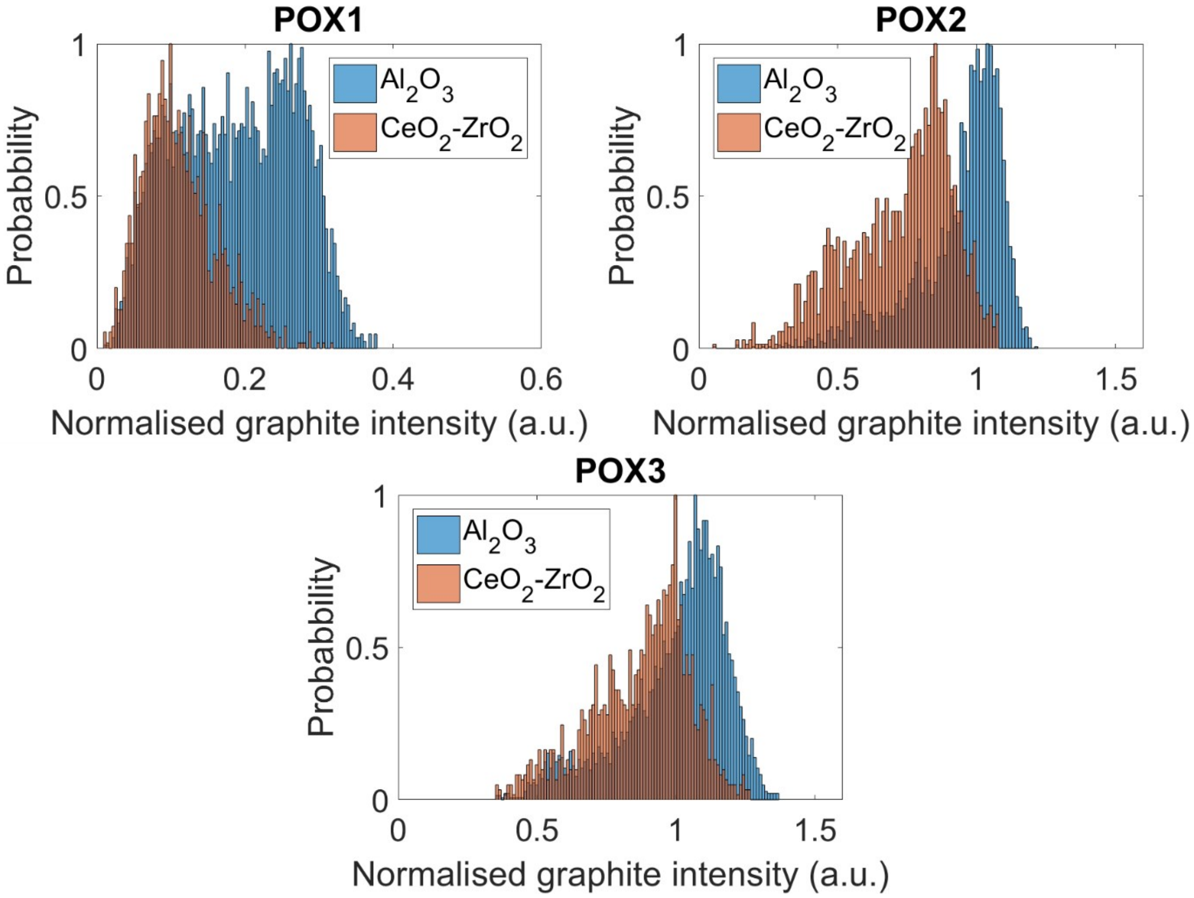

Figure S26. *Histograms describing the distribution of graphite intensity under POX1, POX2 and POX3 reaction conditions for the* Al_2O_3 *and* CeO_2-ZrO_2 *areas.*

7. Physical changes due to coke deposition

3D XRD-CT data were used to perform a quantitative analysis on how the catalyst particles were expanding as a function of applied conditions. Only one catalyst particle was fully present in all 3D-XRD-CT datasets during all the reaction stages (due to particles being moved during the coking process and the initial introduction of gases) and it was shown with white arrow in Figure1 of the main text. For each 3D-XRD-CT dataset we calculated the volume of studied particle (in voxels) and knowing the size of tomographic voxel (40 µm × 40 µm × 40 µm) we could then calculate its volume in real space.

Table S2. *Quantitative measurements of catalyst particle expansion during the POX process.*

Conditions	Fresh catalyst	Reduction	POX1	POX2	Spent catalyst
Particle volume	0.111 mm^3	0.117 mm^3	0.119 mm^3	0.142 mm^3	0.148 mm^3

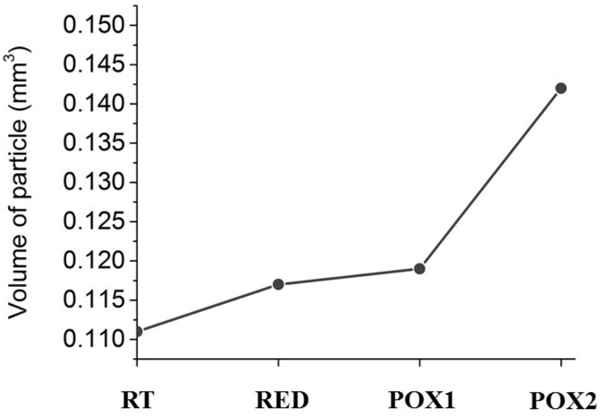

Figure S27. *Expansion of studied particle as a function of experimental conditions (data from Table S2).*

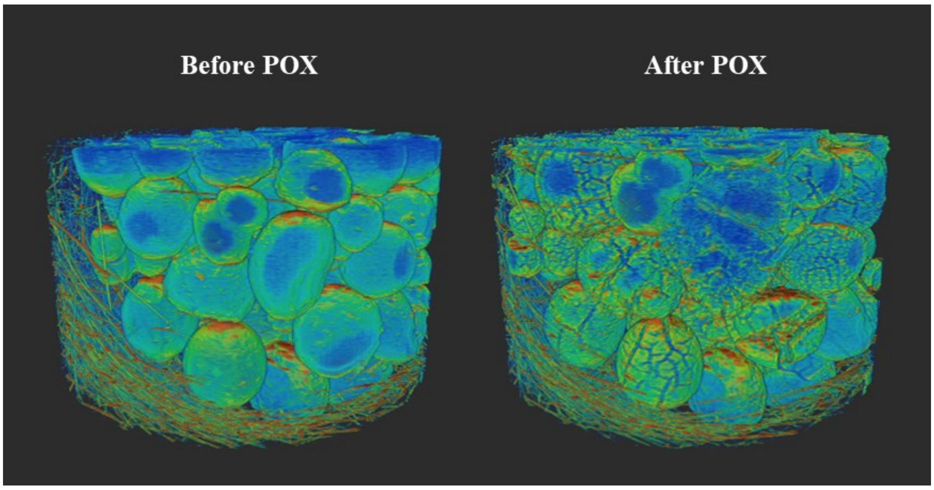

Figure S28. *Absorption-CT images of catalyst collected before and after the POX reaction at the bottom of catalyst rector (reactor inlet). The reactor vessel was masked out from images.*

8. References

(1) Kovarik, L.; Bowden, M.; Shi, D.; Washton, N. M.; Andersen, A.; Hu, J. Z.; Lee, J.; Szanyi, J.; Kwak, J. H.; Peden, C. H. F. Unraveling the Origin of Structural Disorder in High Temperature Transition Al2O3: Structure of θ-Al2O3. *Chem. Mater.* **2015**, *27*, 7042–7049.

(2) Zenou, V. Y.; Fowler, D. E.; Gautier, R.; Barnett, S. A.; Poeppelmeier, K. R.; Marks, L. D. Redox and Phase Behavior of Pd-Substituted (La,Sr)CrO3 Perovskite Solid Oxide Fuel Cell Anodes. *Solid State Ionics* **2016**, *296*, 90–105.

(3) Vamvakeros, A.; Jacques, S. D. M.; Di Michiel, M.; Matras, D.; Middelkoop, V.; Ismagilov, I. Z.; Matus, E. V.; Kuznetsov, V. V.; Drnec, J.; Senecal, P.; et al. 5D Operando Tomographic Diffraction Imaging of a Catalyst Bed. *Nat. Commun.* **2018**, *9* (1), 4751.